Experimental and *ab initio* structural studies of liquid Zr_2Ni

S. G. Hao, M. J. Kramer, C. Z. Wang, K. M. Ho, S. Nandi, A. Kreyssig, and A. I. Goldman
Ames Laboratory, U.S. DOE and Iowa State University, Ames, Iowa 50011, USA

V. Wessels, K. K. Sahu, and K. F. Kelton
Department of Physics, Washington University, Saint Louis, Missouri 63130, USA

R. W. Hyers and S. M. Canepari
University of Massachusetts, Amherst, Massachusetts 01003, USA

J. R. Rogers
NASA Marshall Space Flight Center, Huntsville, Alabama 35812, USA

(Received 10 November 2008; revised manuscript received 31 January 2009; published 20 March 2009)

High-energy x-ray diffraction and *ab initio* molecular-dynamics simulations demonstrate that the short-range order in the deeply undercooled Zr_2Ni liquid is quite nuanced. The second diffuse scattering peak in the total structure factory sharpens with supercooling, revealing a shoulder on the high-Q side that is often taken to be a hallmark of increasing icosahedral order. However, a Voronoi tessellation indicates that only approximately 3.5% of all the atoms are in an icosahedral or icosahedral-like environment. In contrast, a Honeycutt-Andersen analysis indicates that a much higher fraction of the atoms is in icosahedral (15%–18%) or distorted icosahedral (25%–28%) bond-pair environments. These results indicate that the liquid contains a large population of fragmented clusters with pentagonal and distorted pentagonal faces, but the fully developed icosahedral fragments are rare. Interestingly, in both cases, the ordering changes little over the 500 K of cooling. All metrics show that the nearest-neighbor atomic configurations of the most deeply supercooled simulated liquid (1173 K) differ topologically and chemically from those in the stable C16 compound, even though the partial pair distributions are similar. The most significant structural change upon decreasing the temperature from 1673 to 1173 K is an increase in the population of Zr in Ni-centered clusters. The structural differences between the liquid and the C16 increase the nucleation barrier, explaining glass formation in the rapidly quenched alloys.

DOI: 10.1103/PhysRevB.79.104206 PACS number(s): 61.05.cp, 61.20.Ja, 61.25.Mv

I. INTRODUCTION

In recent years there is increased recognition that local atomistic structures of the liquid phases play an important role in dictating the transformation pathways in metallic alloy systems.[1–5] Crystalline, quasicrystalline, or amorphous phases that have short-range and medium-range orders that are similar to that of the corresponding liquid structures generally have smaller interfacial free energies between the amorphous and ordered phases.[3,5–8] This has been proposed to be an influential factor with rapidly cooled liquid metallic alloys not only for the selective nucleation of certain structures among many competing ones but also for avoiding crystallization to form a glass. Therefore, obtaining a more quantitative description of the structure of liquid metal alloys, in particular in their undercooled state, is important for discriminating between various theories of crystal growth and glass formation.

However, reliable structural determination of liquid metallic alloys is not a trivial undertaking.[9] At high temperatures, the crucible choice is crucial and some materials may not be amenable to penetration by neutrons or x-rays typically used for structural determination either wide angle scattering or absorption studies. Levitation techniques[10,11] allow the limitation imposed by crucibles to be bypassed; eliminating reaction concerns and leading to deeper undercoolings then can be achieved in typical castings. Here, we present the results from x-ray scattering experiments using the levitation techniques on an ideal alloy system, Zr_2Ni. Complementary *ab initio* molecular-dynamics (MD) simulations are performed to elucidate the temperature dependence of atomistic structure and short-range order (SRO) in the liquid.

The Zr_2Ni is an ideal model system for combining levitation, scattering, and simulations studies.[12–23] The thermodynamically stable C16 (space group 140, $I4/mcm$) compound melts congruently at 1293 K, so no compositional segregation or peritectic reactions are expected in the deeply undercooled liquid. This composition can be made amorphous by rapid solidification, and a number of research groups have reported partial pair distributions for the glass structures.[24,25] To a first approximation, the amorphous structure should be an extreme limit to the structure of the deeply undercooled liquid and hence provide a reality check for both the experiments and simulations. The vapor pressures of Zr and Ni are low so mass loss should be of little concern in the experiment.[26]

II. EXPERIMENTAL DETAILS

Samples of the appropriate composition were prepared from high-purity low oxygen crystal bar Zr (99.95 at. % metals basis and less than 50 ppm by mass oxygen) and Ni (99.99%); these were arc melted three times to produce ~6 g of a homogeneous alloy ingot. These ingots were subsequently inductively melted in fused silica crucibles and

injection cast into 1.5 mm diameter Cu molds. The ingots were cut into appropriate lengths and remelted in the same arc melter to form ~30 mg spheres, which were about 2 mm in diameter. After each melting step, the samples were weighed; no appreciable change in mass was observed.

Electrostatic levitation (ESL) techniques were combined with high-energy x-ray synchrotron methods as previously described[11,27] but with some modifications. The diffracted high-energy x-rays [129 keV, 0.0958(6)Å] were detected over a Q range of 15 $Å^{-1}$ in 1 s using the GE area detector and averaged over 15 scans, with the sample held at a fixed temperature. A collimator was added to the interior of the chamber after the first window to eliminate scattering from the Be entrance window, and a beamstop was placed outside the exit Be window to eliminate that scattering. Corrections were made for the sample-to-detector distance and its orientation relative to the beam normal using a silicon sphere levitated in the same manner. The $S(Q)$ data were derived from the normalized intensity per atom in electron units following standard procedures[28] using PDFGETX2.[29] The liquid sample volumes were measured as a function of temperature using an optical imaging technique described elsewhere.[30] The volume measurements were calibrated using a NIST traceable WC sphere.

A 32.782 mg sphere of Zr_2Ni was electrostatically levitated and then heated to ~1673 K and radiantly cooled to approximately room-temperature multiple times. In the initial heating step the sample was held at 1673 K for ~90 s; the hold times were 10 to 30 s for the next three subsequent heating cycles. The longer hold time for the initial heating was to evaporate volatile contaminates and melt surface oxides that could act as sites for heterogeneous nucleation during cooling. On the fourth heating cycle the power to the heating laser was reduced during the hold to decrease the temperature by 50–100 K; this temperature was maintained (±5 K) for 20–30 s. During this isothermal hold, 15 complete diffraction patterns were taken with the GE detector described above using an exposure time of 1 s per pattern. These 15 patterns were averaged before applying the standard data corrections described above. Scattering data were collected at successively lower temperatures until recalescence was observed in the pyrometery data, and crystal peaks were observed on the area detector (Fig. 1). Volume measurements were made during the heating and cooling cycles. Since the crystallization of the droplet results in a significant distortion of the sample from a nearly perfect sphere, density measurements are most precise for the liquid phase. Only a 0.02 mg mass loss was measured after the end of the 5 heating/cooling cycles. Subsequent microprobe analysis of the recovered sample showed that the Zr concentration was 66.17 ± 0.27 while the Ni concentration was 33.79 ± 0.27 at. %. The sample remained phase pure based on a Rietveld refinement of the scattering data of the sphere in the crystalline state on heating and cooling. Using this composition, the number density can be directly determined from the measured volume of the liquid droplet. The number density data for the liquid are best fit to a quadratic (R=0.988 atoms/$Å^3$),

$$\rho = -5.75 \times 10^{-10} T^2 - 8.33 \times 10^{-7} T + 0.0534. \quad (1)$$

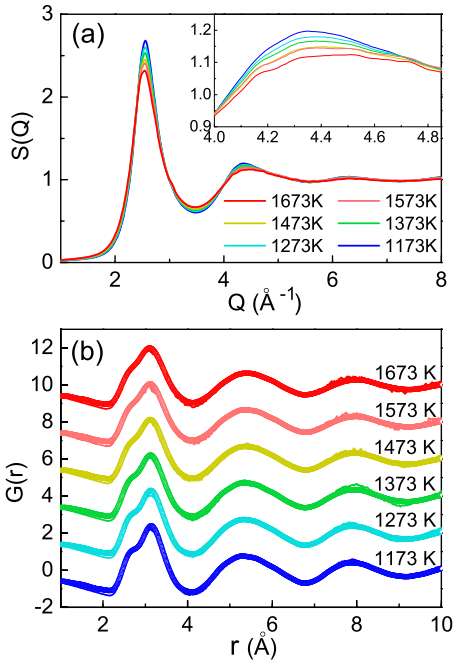

FIG. 1. (Color online) (a) Experimental total scattering factor [$S(Q)$] for the liquid Zr_2Ni alloy. The inset figure shows the detail of the second peak. (b) The reduced distribution function by x-ray (circle) and by *ab initio* MD simulations (line). The pink-dashed line is the MD data of 198 atoms model at T=1573 K. The different scattering factors for Zr and Ni have been included in the simulation data.

III. SIMULATION METHODS

To elucidate the atomistic structure and to investigate the SRO in the liquid, we have performed *ab initio* MD simulations of the liquid as a function of temperature. The simulations were performed within the density-functional theory using a plane-wave basis with the projector augmented-wave (PAW) method accounting for core-valence electron interactions[31,32] and the Perdew-Wang exchange and correlation potential[33] as implemented in VASP.[34–36] The cutoff energy of the plane-wave basis is 270 eV. The system consists of 99 atoms (66 Zr and 33 Ni) in a cubic supercell with periodic boundary conditions. The simulations were carried out in a *NVT* ensemble with Nosé thermostats at six temperatures, from 1673 down to 1173 K. At each temperature, the average pressure of the system was tuned to a value close to zero by changing the size of the supercell. After allowing thermal equilibration at each temperature, the statistics of the structures and properties of the liquids were made over 2000 MD steps (3 fs/step) for the samples above the melting temperature (1293 K) and 5000 MD steps for the undercooled liquids. As a test, we have run an additional 9000 MD steps (totally 14000 MD steps) at 1173 K and 3000 MD steps (totally 5000 MD steps) at 1673 K. Moreover local structure analysis showed almost the same results. Only the Γ point was used to sample the Brillouin zone. Our test simulations with 4k sampling points or a larger simulation cell (of 198 atoms) gave an essentially identical pair-correlation function to the 99 atom Γ point simulation. Microscopically, local

TABLE I. Calculated values for the molten Zr_2Ni alloy. 2000 steps MD for 1673–1373 K and 5000 steps for 1173 and 1273 K.

T (K)	ρ_0 (atoms/Å^3)	$g_{\text{Ni-Ni}}$			$g_{\text{Ni-Zr}}$			$g_{\text{Zr-Zr}}$		
		Position	Height	Width	Position	Height	Width	Position	Height	Width
1173	0.0514	2.5705	1.5164	0.5173	2.6685	2.5969	0.4738	3.2011	2.5068	0.6461
1273	0.0511	2.5675	1.4455	0.5255	2.6665	2.4902	0.4792	3.1967	2.4244	0.6631
1373	0.0511	2.5541	1.4385	0.5297	2.6622	2.3141	0.4850	3.1886	2.3406	0.6714
1473	0.0507	2.5631	1.3392	0.5579	2.6565	2.1800	0.5039	3.1851	2.2568	0.6803
1573	0.0506	2.5463	1.3965	0.5483	2.6542	2.0883	0.5160	3.1819	2.2033	0.6878
1673	0.0506	2.5402	1.3930	0.5491	2.6545	2.0658	0.5275	3.1825	2.1550	0.7068
C16										
1273	0.0527	2.6193	2.4354	0.4906	2.7543	4.5203	0.4829	3.2956	3.1896	0.6592

structure analysis on the test sample of the 198 atom model showed very similar cluster population as the 99 atom model. Since we focus on the local structures of liquid Zr_2Ni the 99 atom model is large enough. We also performed MD simulation for the C16 Zr_2Ni alloy at 1273 K by using 64 Zr and 32 Ni atoms to compare with the liquid.

IV. RESULTS AND DISCUSSION

The experimental $S(Q)$ shows a systematic increase in the intensity of the first and second diffuse scattering peaks as the temperature is reduced from 1673 to 1123 K [Fig. 1(a)]. The sharpening of the second diffuse peak is asymmetric, with the lower-Q side, ~4.3 Å^{-1}, showing a considerable enhancement with decreasing temperature [see inset of Fig. 1(a)]. Such behavior is commonly believed to indicate icosahedral order in transition-metal liquids,[1,37] although recent reverse Monte Carlo studies have indicated that this is likely not always the case.[38–40]

As shown in Table I, the calculated number densities at different temperatures are consistent with the values from Eq. (1) which is fit from experimental data. The error is within less than 0.5%. The reduced atomic distribution function, $G(r)=2/\pi\int_0^\infty Q[S(Q)-1]\sin(Qr)dQ$, obtained by a Fourier transformation of the $S(Q)$ derived from the x-ray scattering data (open circles) compares favorably with the atomic distribution function $[g(r)]$, which is obtained from the *ab initio* MD simulations (lines) at identical temperatures [Fig. 1(b)] and scaled using the computed number density (ρ_0), $G(r)=4\pi r\rho_0[g(r)-1]$. In particular, the development of a shoulder in the nearest-neighbor shell ($r\approx 2.7$ Å) with cooling in the experimental data is well reproduced by the simulations. In binary disordered systems, partial pair correlations can provide useful insights into the chemical ordering. While the experimental determination of the partial pair distribution functions is a difficult and complicated task, requiring anomalous x-ray scattering studies with different wavelengths or neutron studies of samples prepared with isotopic substitution, the calculation of the partial pair-correlation functions from the MD simulation is straightforward. Figure 2 shows the partial pair-correlation function [partial $g(r)$] at different temperatures from our *ab initio* MD simulations. With decreasing temperature, the partial $g(r)$'s become slightly sharper and the shoulder of $G(r)$ [Fig. 1(b)] develops due to an increase in the Ni-Zr and Zr-Zr nearest-neighbor distances [indicated in the $g(r)_{\text{Ni-Zr}}$ and $g(r)_{\text{Zr-Zr}}$ partials shown in Fig. 2 and listed in Table I]. The results of the centroid positions for the first shell partials are similar to those for the Zr_2Ni metallic glass.[24] The partials for the Zr_2Ni liquid and crystalline C16 phase measured at 1273 K show the same relative distributions with short Ni-Ni, intermediate Ni-Zr, and longer Zr-Zr nearest-neighbor distances. Massobrio *et al.*[41] studied amorphization induced by chemical disorder in crystalline Zr_2Ni. The partial correlation functions at 300 K show short Ni-Ni, medium Ni-Zr, and long Zr-Zr bondings as well, consistent with our results. However, second peaks in the partials of our results (high-temperature liquids) are not split, although a trend can be found in $g(r)_{\text{Ni-Ni}}$. In comparison, as shown in the results of Massobrio *et al.*,[41] second peaks of the partials are clearly split into two peaks in the amorphous state of 300 K. As shown in Fig. 2, the centroids of the partials for the C16 phase show slightly larger nearest-neighbor distances and the distributions are narrower (Table I). As expected, the significant differences are for the longer-range correlations, with the sec-

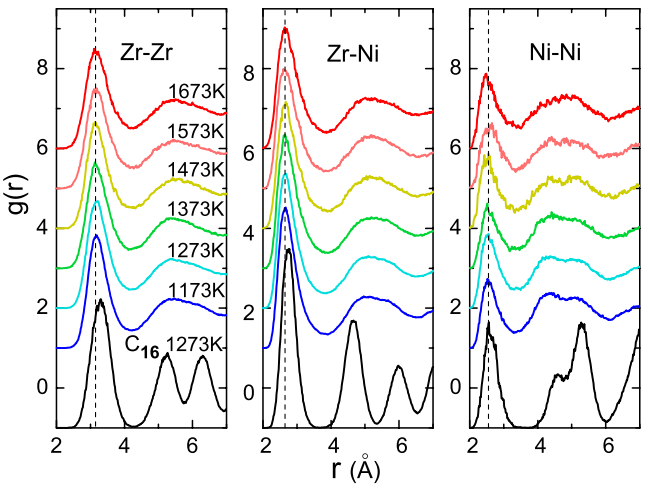

FIG. 2. (Color online) The partial pair-correlation functions by *ab initio* MD simulations. The dashed lines are at the maximum of the pair-correlation functions of the liquids to compare with that of the C16 alloy at 1273 K.

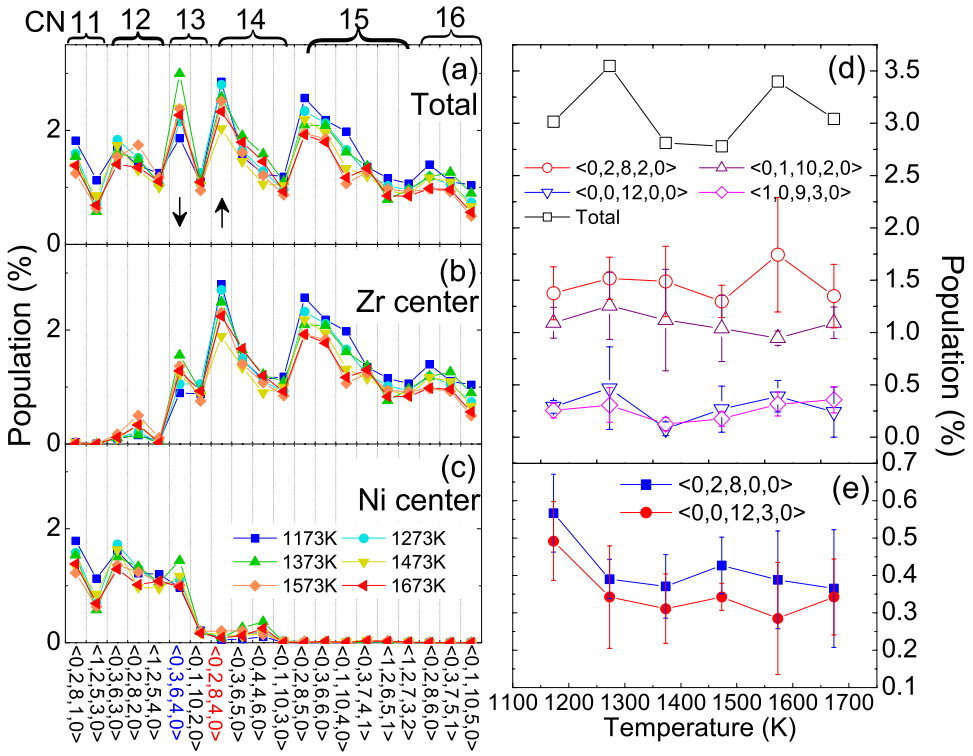

FIG. 3. (Color online) Populations of the 20 most frequent Voronoi indices for (a) total, (b) Zr center, and Ni center (c). The indices are sorted by the CN as shown in the top of the figure. The Voronoi populations of (d) icosahedral and icosahedral-like clusters and (e) C16-like clusters $\langle 0,2,8,0,0\rangle$ and $\langle 0,0,12,3,0\rangle$ as a function of temperature.

ond shells in the 1173 K liquid starting to show more definition between 4 and 6 Å (Fig. 2). The shifting of the liquid partials to shorter distances than those of the crystalline compound illustrates that locally there are regions in the liquid that are more densely packed than the C16 structure, even though the number density of crystalline solid is higher than the liquid, 5.26×10^{-2} vs 5.14×10^{-2} atoms/Å^3, respectively. This is a natural consequence of the inherent disorder of the liquid leading to inefficient packing.

The presence of significant icosahedral order is often cited as an important precursor for glass formation[42–45] and is believed to be responsible for the deep undercooling of liquid metals.[46] It would be interesting to quantitatively investigate how much local fivefold order or, more specifically, icosahedral clusters are presented in Zr_2Ni liquids and whether they become more dominant as the liquid is undercooled, as has been argued in other transition metal and alloy liquids.[1,37,47–49] Given that the simulations are so well matched to the experimental data, we can put a high degree of confidence on the partial pair correlation determined by the MD simulations to provide an accurate description of the SRO of the liquid and how it changes with undercooling. A commonly used method for describing the local structure of a disordered system is a Voronoi tessellation.[50–53] In this method, a coordination polyhedron surrounding a center atom can be differentiated by specific Voronoi indices $\langle n_i\rangle$. Here n_i denotes the number of i-edged faces of the Voronoi polyhedron and $\Sigma_i n_i$ is the coordination number (CN) of the center atom in the polyhedron. The number of edges of each polyhedral face denotes the number of common neighbors shared by the center atom and one of its neighboring atoms. Here we set $i=3$, 4, 5, 6, and 7.

The Voronoi tessellation analysis shows that the CN distributions are weakly temperature dependent with a maximum of CN$\approx$14. A comparison of the populations of the 20 most abundant Voronoi indices at all temperatures is shown in Fig. 3. The $\langle 0,3,6,4,0\rangle$, $\langle 0,2,8,4,0\rangle$, and $\langle 0,2,8,5,0\rangle$ are the three most abundant polyhedra in the liquid. These clusters are primarily Zr centered and are not icosahedral or icosahedral-like clusters. The Zr-centered clusters prefer a higher CN, $\geq$13 [Fig. 3(b)], while Ni-centered clusters prefer a lower CN, $<$13 [Fig. 3(c)]. The populations of polyhedra with CN of 11, 15, and 16 generally increase as the temperature of the liquid is decreased, while the behavior of those with CN between 12 and 14 is mixed. For example, the population of the $\langle 0,3,6,4,0\rangle$ clusters initially increases with cooling from 1673 to 1373 K (which is above the melting temperature) but dramatically decreases upon undercooling to 1173 K, as indicated by the downward arrow in Fig. 3(a). The behavior of the $\langle 0,2,8,4,0\rangle$ is opposite to that of $\langle 0,3,6,4,0\rangle$, as indicated by the upward arrow in Fig. 3(a). It is interesting to note that the number of ideal icosahedral polyhedra, $\langle 0,0,12,0,0\rangle$, is small, less than 0.5% for all temperatures, even though polyhedra with pentagonal faces are common ($\sim$45%). Expanding to include all icosahedral-like clusters, $\langle 0,0,12,0,0\rangle$, $\langle 0,2,8,2,0\rangle$, $\langle 0,1,10,2,0\rangle$, and $\langle 1,0,9,3,0\rangle$, the contribution is still less than 3.5% [Fig. 3(d)].

In addition to a Voronoi tessellation analysis, other metrics that are commonly used to characterize the local struc-

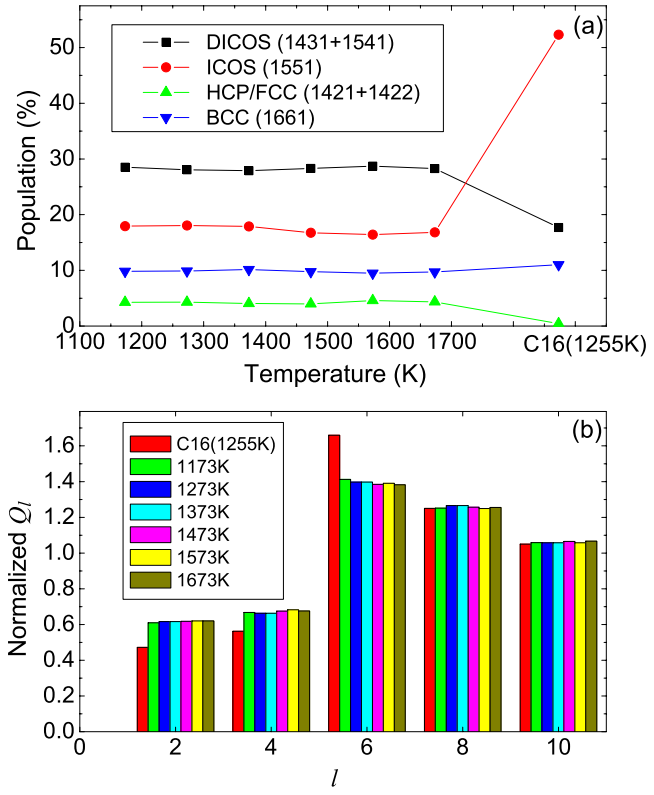

FIG. 4. (Color online) (a) A HA index analysis of the liquid, showing little change with temperature; the HA for the liquid is very different from that for the C16 at 1255 K. DICOS indicates a distorted icosahedral and ICOS indicates icosahedral bond pairs. (b) BOO analysis of the liquid also shows little change with temperature. As for the HA analysis, the BOO for the liquid is quite different from that for the C16 phase, indicating different local structures. Q_l is normalized such that $\Sigma_{\text{even } l} Q_l = 5$, characteristics of random configuration.

tures of liquids and glasses include the Honeycutt-Andersen (HA) index[54] and the bond orientational order (BOO) parameter[55] analyses. The HA indices are constructed by taking in turn each pair of atoms within a defined cutoff distance in the total ensemble of atoms as a *root pair*. The local structures around these pairs are described by four indices that denote (1) to which peak in $g(r)$ the pair belongs, (2) how many atoms are counted as nearest neighbors of the root pair, (3) the number of pairs of these nearest neighbors that are close enough to form a bond, and (4) a classification for clusters with identical sets of the first three indices but with different bond arrangements. For the BOO parameter analysis a set of order parameters expressed in terms of spherical harmonics, $Q_{lm}(\boldsymbol{r}) = Y_{lm}[\theta(\boldsymbol{r}), \varphi(\boldsymbol{r})]$, are associated with the orientation of each pair of atoms, providing information that is similar to that for the Voronoi analysis. The results of the HA index analysis are shown in Fig. 4(a). Root pairs of atoms that have nearest neighbors in an icosahedral configuration are indicated by the 1551 index; distorted icosahedral root pairs are reflected in the 1431 and 1541 indices. As observed in Fig. 4(a), the liquid structure is primarily characterized by distorted icosahedral order (~28% of the local configurations). While the icosahedral order is less (~18% of the local configurations), it is considerably larger than indicated by the Voronoi tessellation analysis (~0.5%). The results of the BOO analysis are shown in Fig. 4(b). An icosahedral cluster would show a large value of Q_6, while the values of other indices would be nearly zero.[55] Although the value of Q_6 is slightly larger, the values of $Q8$ and $Q10$ are similar, reflecting a predominance of nonicosahedral local order similar to the conclusions reached from the Voronoi tessellation analysis.

Why do these different metrics give such different values regarding the prominence of local icosahedral order? Both the Voronoi and BOO analyses provide information that reflects the full three-dimensional (3D) nearest-neighbor environment around each atom. In contrast, the HA index analysis provides a measure of the topology of only those atoms that are nearest neighbors to a given pair of atoms (root pair), essentially reflecting the symmetry of the faces of the polyhedral nearest-neighbor clusters. In agreement with this interpretation, the percentage of HA indices for icosahedral and distorted icosahedral environments around root pairs (~46%) is nearly identical to the percentage of pentagonal faces on the Voronoi polyhedra (~45%). This suggests that while many pairs of atoms sit in an icosahedral or distorted icosahedral local environment, the number of fully developed icosahedral clusters is rare. More significantly, all three methods indicate a negligible change in the short-range order with decreasing temperature, unlike the behavior previously reported in other transition-metal alloys.

It is interesting to ask whether the local structure of the liquid favors the nucleation of the stable compound, especially since the partial pair distributions are similar. In the ideal C16 Zr_2Ni structure, two thirds of the polyhedra are Zr centered $\langle 0,0,12,3,0\rangle$ with 11 Zr and 4 Ni neighbors, and one third are Ni centered $\langle 0,2,8,0,0\rangle$ with eight Zr and two Ni neighbors. In the liquid state, as indicated in Fig. 3(e), both indices comprise less than 0.6% of the total. While these two indices are rare in the liquid their population does increase, from 0.37% to 0.57% for $\langle 0,2,8,0,0\rangle$ and from 0.34% to 0.49% for $\langle 0,0,12,3,0\rangle$ as the temperature decreases from 1673 to 1173 K. However, the population of $\langle 0,2,8,0,0\rangle$ is always larger than that of $\langle 0,0,12,3,0\rangle$, in contrast to the 1:2 ratio in the C16 structure. The HA and BOO indices are also different in the undercooled liquid and the C16 structures [Figs. 4(a) and 4(b)]; it is interesting that the 1551 HA index for the C16 is very large, reflecting the polytetrahedral order in that phase. In agreement with the Voronoi analysis, however, the liquid and C16 structures are very different.

Looking more closely at the local chemical environments, we find that Zr atoms prefer ten Zr neighbors and five Ni neighbors, i.e., at 1673 K (10:5) is ~8.5% of total population while (11:4) is 8.2% of the total. Ni atoms prefer ten Zr neighbors and 2 Ni neighbors, i.e., at 1673 K (10:2) is ~9.0% of total population while (8:2) is only 1.4%. The chemical environment around the Zr atoms does not show any distinct trend with decreasing temperature. On the other hand, the populations of Ni centers with (7:5) and (8:5) neighbors decrease (as much as 2.2%) while the populations of (9:3) and (9:2) neighbors increase (as much as of 5%) from 1673 to 1173 K (Fig. 5). The increase in the (9:3)

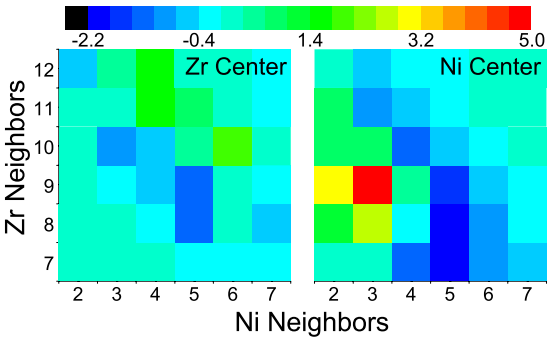

FIG. 5. (Color online) The population difference of the local chemical distributions of the Zr and Ni clusters between $T=1173$ and 1673 K. The blue square indicates the decrease in population, while the red one indicates the increase in population, e.g., for the Zr-centered cluster with eight Zr neighbors and five Ni neighbors, (8:5), the population decreases ~1.1%, and for the Ni-centered cluster with nine Zr neighbors and three Ni neighbors, (9:3), the population increases ~5.0%, when temperature decreases from 1673 to 1173 K.

Ni-centered clusters from 9% to 14% is the most significant change, indicating that as the liquid is undercooled, the number of Zr atoms surrounding Ni atoms substantially increases. The local chemical order is actually determined by the Helmholtz free energy and the distribution of local chemical order is dependent on temperature as well as the Helmholtz free energy, as discussed in the appendix of Ref. 56. In comparison with local chemistry in liquids, the C16 Zr_2Ni alloy distribution are (11:4) for Zr atoms and (8:2) for Ni atoms. Thus for the undercooled liquid, the local Ni chemistry moves substantially toward that of the C16 Zr_2Ni alloy. This trend is also seen in the decrease in height of the $g(r)_{\text{Ni-Ni}}$, while the $g(r)_{\text{Zr-Zr}}$ height increases with undercooling. However, the local chemistry in the undercooled liquid is still significantly different from that of the C16 crystalline structure. Both the topology and chemistry of the C16 and liquid phases are, therefore, different. Since the scattering data show that only the C16 phase forms from this liquid, we surmise that it is topological and chemical difference is responsible for the nucleation barrier and likely underlies easy glass formation.

V. CONCLUSIONS

In summary, while developing local icosahedral order in liquids is often invoked to explain the deep undercoolings and the propensity of some metallic alloys to form amorphous solids, it is not necessarily universal. Our simulations show that while a high percentage of fragmented icosahedral root pairs exists in undercooled liquids of Zr_2Ni, complete 3D icosahedral clusters are rare. Yet, this liquid alloy will form a glass when rapidly cooled. Further, we find that even though the first shell partial pair-correlation functions of the liquid and crystalline solid are similar, i.e., short Ni-Ni, intermediate Ni-Zr, and long Zr-Zr bonds, the local chemical environment is quite different between the liquid and the C16 crystalline phase. These topological and chemical differences give rise to a high nucleation barrier for the C16 phase. The chemical environment around the Ni atoms must undergo considerable topological reordering before the C16 phase can form. The simulations show that while the local chemistry around the Ni atoms in the deeply undercooled liquid is tending toward that found in the C16 structure, less than 0.6% of the clusters in the 1173 K liquid are topologically similar to those in the stable compound. The dissimilarity between the liquid and the ordered phase makes it difficult to nucleate the C16 and explain glass formation in this alloy. These experimentally validated MD simulations of the deeply undercooled liquid provide a first step toward determining the distribution and relative stability of topologically stable clusters, which will enable more accurate modeling of the nucleation and growth of the stable structures.

ACKNOWLEDGMENTS

Ames Laboratory is operated for the U.S. Department of Energy by Iowa State University under Contract No. DE-AC02-07CH11358. This work was supported by the Director for Energy Research, Office of Basic Energy Sciences, including a grant of computer time at the National Energy Research Supercomputing Center (NERSC) in Berkeley. The high-energy x-ray work at the MUCAT sector of the APS was supported by the Office of Science, Basic Energy Sciences, U.S. Department of Energy under Contract No. DE-AC02-06CH11357. The work at Washington University was partially supported by the National Science Foundation under Grant No. DMR-0606065 and by NASA under Contract No. NNM04AA016.

[1] K. F. Kelton, G. W. Lee, A. K. Gangopadhyay, R. W. Hyers, T. J. Rathz, J. R. Rogers, M. B. Robinson, and D. S. Robinson, Phys. Rev. Lett. **90**, 195504 (2003).
[2] D. Holland-Moritz, T. Schenk, V. Simonet, R. Bellissent, P. Convert, T. Hansen, and D. M. Herlach, Mater. Sci. Eng., A **A375-A377**, 98 (2004).
[3] G. W. Lee, A. K. Gangopadhyay, T. K. Croat, T. J. Rathz, R. W. Hyers, J. R. Rogers, and K. F. Kelton, Phys. Rev. B **72**, 174107 (2005).
[4] K. F. Kelton, A. K. Gangopadhyay, T. H. Kim, and G. W. Lee, J. Non-Cryst. Solids **352**, 5318 (2006).
[5] D. Holland-Moritz, T. Schenk, V. Simonet, and R. Bellissent, Philos. Mag. **86**, 255 (2006).
[6] J. C. Holzer and K. F. Kelton, Acta Metall. Mater. **39**, 1833 (1991).
[7] D. Holland-Moritz, Int. J. Non-Equilib. Process. **11**, 169, (1998).
[8] D. T. Wu, L. Granasy, and F. Spaepen, MRS Bull. **29**, 945 (2004).
[9] L. Hennet, S. Krishnan, A. Bytchkov, T. Key, D. Thiaudiere, P. Melin, I. Pozdnyakova, M. L. Saboungi, and D. L. Price, Int. J.

Thermophys. **26**, 1127 (2005).
[10] G. Mathiak, I. Egry, L. Hennet, D. Thiaudiere, I. Pozdnyakova, and D. L. Price, Int. J. Thermophys. **26**, 1151 (2005).
[11] A. K. Gangopadhyay, G. W. Lee, K. F. Kelton, J. R. Rogers, A. I. Goldman, D. S. Robinson, T. J. Rathz, and R. W. Hyers, Rev. Sci. Instrum. **76**, 073901/1 (2005).
[12] K. Ohsaka, S. K. Chung, and W. K. Rhim, Acta Mater. **46**, 4535 (1998).
[13] X.-d. Wang, M. Qi, and C. Dong, Mater. Sci. Eng., A **A375-A377**, 701 (2004).
[14] K. N. Lad and A. Pratap, Physica B **334**, 135 (2003).
[15] X.-d. Wang, M. Qi, and C. Dong, J. Non-Cryst. Solids **318**, 142 (2003).
[16] A. A. Turchanin, M. A. Turchanin, and P. G. Agraval, Mater. Sci. Forum **360-362**, 481 (2001).
[17] A. A. Turchanin and I. A. Tomilin, Ber. Bunsenges. Phys. Chem. **102**, 1252 (1998).
[18] T. Aihara, Jr., Y. Kawazoe, and T. Masumoto, J. Non-Cryst. Solids **205-207**, 875 (1996).
[19] R. T. Savalia, R. Tewari, G. K. Dey, and S. Banerjee, Acta Mater. **44**, 57 (1996).
[20] D. K. Lee and K. S. Park, Taehan Kumsok Hakhoechi **31**, 1043 (1993).
[21] J. C. Barbour, M. Nastasi, and J. W. Mayer, Appl. Phys. Lett. **48**, 517 (1986).
[22] J. C. Barbour, Phys. Rev. Lett. **55**, 2872 (1985).
[23] T. Mizoguchi, N. Nishioka, T. Suemasa, S. Yoda, N. Akutsu, H. Narumi, T. Kudo, M. Akimitsu, N. Watanabe, M. Nishi, and K. Motoya, J. Phys. (France) **43**, 659 (1982).
[24] T. Fukunaga, K. Itoh, T. Otomo, K. Mori, M. Sugiyama, H. Kato, M. Hasegawa, and A. Hirata, Intermetallics **14**, 893 (2006).
[25] T. Fukunaga, D. Touya, K. Itoh, T. Otomo, K. Mori, H. Kato, and M. Hasegawa, J. Metastable Nanocryst. Mater. **2425**, 217 (2005).
[26] R. E. Honig and D. A. Kramer, RCA Rev. **30**, 285 (1969).
[27] A. J. Rulison, J. L. Watkins, and B. Zambrano, Rev. Sci. Instrum. **68**, 2856 (1997).
[28] T. Egami and S. J. L. Billinge, in *Underneath the Bragg Peaks: Structural Analysis of Complex Materials*, edited by R. W. Cahn (Pergamon Elsevier, Oxford, U.K., 2003).
[29] I. K. Jeong, J. Thompson, T. Proffen, A. M. P. Turner, and S. J. L. Billinge, J. Appl. Crystallogr. **34**, 536 (2001).
[30] R. C. Bradshaw, D. P. Schmidt, J. R. Rogers, K. F. Kelton, and R. W. Hyers, Rev. Sci. Instrum. **76**, 125108 (2005).
[31] P. E. Blochl, O. Jepsen, and O. K. Andersen, Phys. Rev. B **49**, 16223 (1994).
[32] G. Kresse and D. Joubert, Phys. Rev. B **59**, 1758 (1999).
[33] Y. Wang and J. P. Perdew, Phys. Rev. B **43**, 8911 (1991).
[34] G. Kresse, J. Non-Cryst. Solids **192-193**, 222 (1995).
[35] G. Kresse and J. Furthmuller, Phys. Rev. B **54**, 11169 (1996).
[36] G. Kresse and J. Furthmuller, Comput. Mater. Sci. **6**, 15 (1996).
[37] T. Schenk, D. Holland-Moritz, V. Simonet, R. Bellissent, and D. M. Herlach, Phys. Rev. Lett. **89**, 075507 (2002).
[38] T. H. Kim, G. W. Lee, A. K. Gangopadhyay, R. W. Hyers, J. R. Rogers, A. I. Goldman, and K. F. Kelton, J. Phys.: Condens. Matter **19**, 455212 (2007).
[39] T. H. Kim and K. F. Kelton, J. Chem. Phys. **127**, 079902 (2007).
[40] K. F. Kelton, J. Alloys Compd. **434**, 115 (2007).
[41] C. Massobrio, V. Pontikis, and G. Martin, Phys. Rev. Lett. **62**, 1142 (1989); Phys. Rev. B **41**, 10486 (1990).
[42] H. Tanaka, J. Phys.: Condens. Matter **15**, L491 (2003).
[43] H. J. Lee, T. Cagin, W. L. Johnson, and W. A. Goddard, J. Chem. Phys. **119**, 9858 (2003).
[44] T. Egami, J. Non-Cryst. Solids **353**, 3666 (2007).
[45] X. K. Xi, L. L. Li, B. Zhang, W. H. Wang, and Y. Wu, Phys. Rev. Lett. **99**, 095501 (2007).
[46] F. C. Frank, Proc. R. Soc. London, Ser. A **215**, 43 (1952).
[47] D. Holland-Moritz, T. Schenk, R. Bellissent, V. Simonet, K. Funakoshi, J. M. Merino, T. Buslaps, and S. Reutzel, J. Non-Cryst. Solids **312**, 47 (2002).
[48] D. Holland-Moritz, T. Schenk, V. Simonet, R. Bellissent, P. Convert, and T. Hansen, J. Alloys Compd. **342**, 77 (2002).
[49] A. Di Cicco, A. Trapananti, and S. Faggioni, Phys. Rev. Lett. **91**, 135505 (2003).
[50] J. L. Finney, Proc. R. Soc. London, Ser. A **319**, 495 (1970).
[51] J. L. Finney, Nature (London) **266**, 309 (1977).
[52] V. A. Borodin, Philos. Mag. A **79**, 1887 (1999).
[53] V. A. Borodin, Philos. Mag. A **81**, 2427 (2001).
[54] J. D. Honeycutt and H. C. Andersen, J. Phys. Chem. **91**, 4950 (1987).
[55] P. J. Steinhardt, D. R. Nelson, and M. Ronchetti, Phys. Rev. Lett. **47**, 1297 (1981).
[56] A. B. Bhatia and D. E. Thronton, Phys. Rev. B **2**, 3004 (1970).